

Analytical characterization of adhering vesicles

C. Tordeux and J.-B. Fournier

*Laboratoire de Physico-Chimie Théorique, E. S. P. C. I.,
10 rue Vauquelin, F-75231 Paris cedex 05, France*

P. Galatola

*LBHP, Université Paris 7—Denis Diderot, Case 7056,
2 place Jussieu, F-75251 Paris cedex 05, France*

(Dated: February 1, 2008)

We characterize vesicle adhesion onto homogeneous substrates by means of a perturbative expansion around the infinite adhesion limit, where curvature elasticity effects are absent. At first order in curvature elasticity, we determine analytically various global physical quantities associated with adhering vesicles: height, adhesion radius, etc. Our results are valid for adhesion energies above a certain threshold, that we determine numerically. We discuss the haptotactic force acting on a vesicle in the limit of weak adhesion gradients. We also propose novel methods for measuring adhesion energies and we suggest a possible way of determining the size of suboptical vesicles using controlled adhesion gradients.

PACS numbers: 87.16.Dg, 68.35.Np, 68.03.Cd

I. INTRODUCTION

When phospholipids are dissolved in an aqueous solution, almost all the molecules condensate into bilayers. Lipid bilayers are formed by two contacting monolayers of opposite orientation, in which the hydrophilic heads of the molecules are located at the sides of the structure, the hydrophobic tails being shielded from contact with water [1]. As there is a prohibitive energy cost associated with their free borders, these bilayers form closed objects, which are called vesicles. For some biological studies, vesicles are used as models of the membrane of living cells [2]. They also have applications as encapsulation vectors for drug delivery [3]. Their efficiency as drug delivery vectors is linked to their permeability, which can be affected by adhesion phenomena [4]. Vesicle adhesion on a solid substrate, followed by its rupture and fusion, also provides a simple technique for obtaining supported membranes [5] that can be used for the design of biosensors [6].

Adhesion phenomena between a lipid bilayer and a substrate can be divided into two categories: i) specific adhesion between a particular host protein and a receptor on the substrate [7]; this kind of adhesion generally implies a process of molecular recognition between a receptor and a ligand, and is common in biological systems. ii) non-specific adhesion between the membrane's lipids and the substrate, mediated by universal interactions, e.g., van der Waals forces. Here, we focus on non-specific adhesion, which can be described by an adhesion potential W that represents the free energy gain per unit area of contact. Typical values of W range from 10^{-4} mJ/m² to 1 mJ/m² [8]. Note that the description of adhesion using a contact potential is approximate, because van der Waals forces are actually long-ranged and because membranes may fluctuate in the vicinity of the substrate: adhering vesicles actually never strictly come into contact

with their substrate. Membrane-substrate separations range from 1 nm for the strongest values of W [6], to about 50 nm for the weakest adhesions [9]. The highest values of W tend to produce vesicle rupture during the adhesion process [5], owing to a strong tension induced in the membrane [8].

To determine the shape and free energy of an adhering vesicle, one must take into account the competition between: i) the adhesion energy gain, ii) the constraints on the total membrane area A and the total enclosed volume V , and iii) the free energy cost associated with the curvature elasticity of the membrane. The latter is described by a free energy density proportional to the square of the local mean curvature [10]. For lipids, the corresponding bending rigidity κ is of the order of 10^{-19} J $\simeq 25 k_B T$ at room temperature [11]. Refined vesicle models take into account a constraint on the difference between the areas of the two monolayers [12], or an elasticity associated with it [13]. Physically, this arises from the fact that lipids are not significantly exchanged between the two monolayers during typical experimental times. It is not known at the present time whether this constraint is significant for adhering vesicles: to simplify, we shall disregard it in our approach.

The shapes of axisymmetric adhering vesicles can be determined by functional minimization [8, 14]. However, due to non-linearities in the equilibrium equations, exact solutions can only be determined numerically. In the asymptotic case of infinitely strong adhesion, $W \rightarrow \infty$ (or equivalently $\kappa \rightarrow 0$), the problem is easily solved analytically [14]: the equilibrium shapes are spherical caps, whose features are dictated by the geometrical constraints only. In this paper we characterize the adhesion of vesicles in the case of strong but finite adhesion, by extracting analytical corrections with respect to the infinite adhesion case. We determine analytically the first-order corrections to various physical observables and we dis-

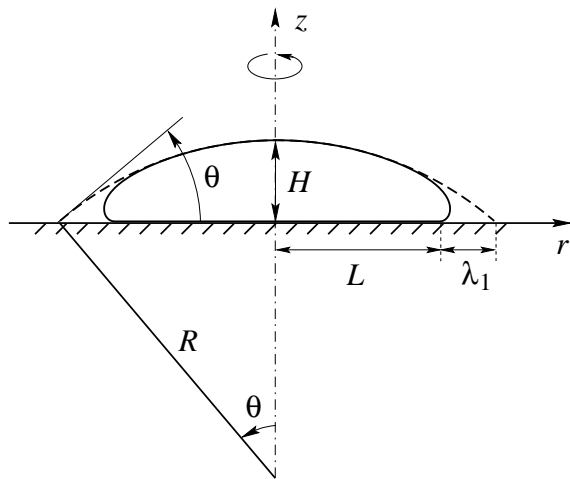


FIG. 1: Definition of the global observables associated with an axisymmetric adhering vesicle. The vesicle's shape, which was calculated numerically, corresponds to a rather deflated situation in which the “contact angle region” is broad and not well-defined. When adhesion is stronger, the vesicle's shape resembles a spherical cap (dashed line), with a strongly curved rim at the foot of the “contact angle” (no discontinuity of the membrane's normal).

cuss their limit of validity by a direct comparison with exact numerical results.

The first-order corrections with respect to the infinite adhesion limit originate from the existence of a strongly curved region at the border of the adhesion disc (see Fig. 1). We shall refer to this region as the “contact angle region”, by analogy with wetting phenomena [15]. The shape of this region has been determined in Refs. [16, 17] using an open membrane description, i.e., no volume constraint and an externally imposed tension acting along a fixed direction mimicking the asymptotic contact angle. Imposing explicitly the volume constraint, we recover the same shape for the contact angle region. The novelty of our approach resides in the analytical description of the various observables associated with the adhering vesicle (height, radius of adhesion, ...).

Standard measurements of adhesion potentials W are based on the determination of the shape of the contact angle region, e.g., by Reflection Interference Contact Microscopy (RICM). Indeed, the radial curvature c of a detaching membrane yields W through the equilibrium relation $c = \sqrt{2W/\kappa}$ [14, 18, 19]. In practice, it is difficult to precisely measure c , and it is more efficient to fit the contact angle region using RICM [17, 20]. Available models rest however on linearized equations for contact angles close to π [17]. Our non-linear analysis allows not only to fit the contact-angle region and determine contact potentials even for contact angles far from π , but also provides new means of determining W by measuring the various global observables.

Our paper is organized as follows: In Sec. II, we introduce the model used to describe the elasticity of vesicles

and their adhesion onto homogeneous substrates. We also define various global observables relevant to the adhesion geometry. Section III contains the results of our analytical calculations: in Sec. III A, we recall the asymptotic limit of infinite adhesion; in Sec. III B, we recall the general equations describing the equilibrium shapes of adhering axisymmetric vesicles; in Sec. III C 1 we calculate the shape of the contact angle region at first-order in $\sqrt{\kappa/(WA)}$; in Sec. III C 2, we determine the contact angle extrapolation length [17, 20]; in Sec. III C 3, we determine the first-order expansions, in power series of $\sqrt{\kappa/(WA)}$, of the various global observables associated with the vesicle's shape; in Sec. III C 4, we calculate at first-order the free energy of adhering vesicles and we discuss haptotaxis (motion induced by an adhesion gradient) [21]. In Sec. IV, we determine *numerically* the global observables and we discuss the range of validity of the corresponding first-order expansions. Finally, in Sec. V, we summarize our results and we discuss some possible applications, including new methods for measuring W .

II. DESCRIPTION OF ADHERING VESICLES

In most experimental situations, although vesicles are slightly permeable to water, their volume V is strongly fixed by the osmotic pressure of the various solubilized ions to which the membrane is impermeable [8]. We shall suppose that this volume constraint remains satisfied for adhering vesicles. The area A of vesicles is also fixed to a high accuracy: solubilized lipids are almost inexistent and the area-stretching modulus k_s , which is of the order of $100 \text{ mJ/m}^2 \gg W$, cannot significantly affect the area constraint [8]. It is traditional to introduce a dimensionless parameter v , the reduced volume, defined by

$$v = \frac{V}{\frac{4}{3}\pi (A/4\pi)^{3/2}}. \quad (1)$$

This quantity $0 < v \leq 1$ describes how much the vesicle is deflated with respect to a sphere ($v = 1$). Due to the constraints, it is fixed.

V and A being fixed, the free energy of an adhering vesicle is given by

$$F = -WA_{\text{adh}} + \oint dA \frac{1}{2} \kappa (c_1 + c_2)^2, \quad (2)$$

where c_1 and c_2 are the two local principal curvatures of the membrane, κ is the Helfrich bending constant [10], A_{adh} is the area of contact between the vesicle and the substrate, and W is the contact potential. As discussed in the Introduction, we simply model the adhesion by an energy proportional to the contact area. In principle, F should also contain a Gaussian curvature term $\bar{\kappa} c_1 c_2$, however we discard it since its integral over the membrane is constant for a given vesicle topology, according to the Gauss-Bonnet theorem [22]. Therefore, there are

only two dimensionless parameters in the problem: v and $\kappa/(WA)$.

In the whole paper, we shall restrict ourselves to axisymmetric vesicle shapes. We define the following global observables (see Fig. 1): we call H the height of the vesicle measured on the revolution axis, and L the radius of the adhesion disc. The adhering area is thus $A_{\text{adh}} = \pi L^2$. In the regime of strong adhesion, vesicles almost take the shape of a spherical cap. In order to precisely define a “contact angle” even in the case of weaker adhesion, we introduce the sphere which is osculatory to the membrane at the point intersecting the revolution axis. We call R its radius and θ the angle at which it intersects the substrate (see Fig. 1). Finally, we define the extrapolation length λ_1 as the distance between the point where the vesicle detaches from the substrate and the intersection between the osculatory sphere and the substrate.

We shall denote throughout by the index zero all the quantities referring to the limit $W \rightarrow \infty$, where the vesicle exactly takes the shape of a spherical cap. Therefore H_0 , R_0 , θ_0 and L_0 are the height, radius, contact angle, and adhesion radius of the corresponding spherical cap.

III. ANALYTICAL RESULTS

Strong adhesion corresponds to the situation where the adhesion energy gain is very large compared to the elastic energy of the vesicle. Since the energy of freely floating vesicles is of order κ [8], even for deflated vesicles, this condition can be expressed as

$$WA \gg \kappa. \quad (3)$$

It corresponds, for a given vesicle, to strong enough contact potentials W , or, for a given W , to large enough vesicles. In this situation, elasticity can be treated as a first-order correction with respect to the asymptotic limit of infinite adhesion. We shall therefore first review the limit $W \rightarrow \infty$ [14].

A. Infinite contact potential W

In this case, adhesion is the only relevant contribution to the free energy of the system, and v is the only dimensionless parameter of the problem. Taking into account the two geometrical constraints, and formally setting $\kappa = 0$, the shape of the adhering vesicle is deduced from the minimization of the following functional:

$$F_0^* = -WA_{\text{adh}}^0 + \Sigma_0 A + P_0 V. \quad (4)$$

Σ_0 is the Lagrange multiplier associated with the area constraint and P_0 is the Lagrange multiplier associated with the volume constraint. Equation (4) can be rewritten as

$$F_0^* = (\Sigma_0 - W) A_{\text{adh}}^0 + \Sigma_0 (A - A_{\text{adh}}^0) + P_0 V. \quad (5)$$

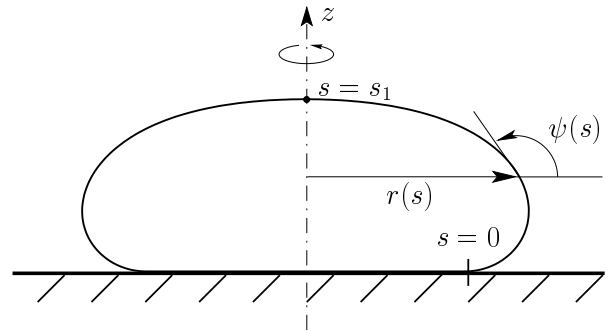


FIG. 2: Definition of the parameters used in the determination of the equilibrium shape of an adhering vesicle.

This functional is identical to that of a liquid droplet wetting a flat substrate, with the correspondence $\Sigma_0 - W \rightarrow \gamma_{\text{SL}} - \gamma_{\text{SV}}$, $\Sigma_0 \rightarrow \gamma_{\text{LV}}$ and $P_0 \rightarrow -\Delta P$, in which γ_{SL} , γ_{SV} , γ_{LV} have their usual meaning and ΔP is the drop’s excess pressure [15]. This implies that infinitely strongly adhering vesicles and liquid droplets have the same ensemble of equilibrium shapes, although they are described by different sets of physical parameters. Consequently, the equilibrium shapes in the asymptotic limit $W \rightarrow \infty$ are spherical caps.

The major physical difference with the case of liquid droplets is that the contact angles are not fixed by surface tensions, but rather by the geometrical constraints acting on the vesicles. The relation between the contact angle θ_0 and the reduced volume v [Eq. (1)] can easily be deduced from simple geometry [8]:

$$v = \frac{8 - 9 \cos \theta_0 + \cos 3\theta_0}{2 (2 - 2 \cos \theta_0 + \sin^2 \theta_0)^{3/2}}. \quad (6)$$

As for the two Lagrange multipliers, they can easily be found by using the analogy with wetting droplets: the Young relation $\gamma_{\text{LV}} \cos \theta + \gamma_{\text{SL}} = \gamma_{\text{SV}}$ yields

$$\Sigma_0 = \frac{W}{1 + \cos \theta_0}, \quad (7)$$

and the Laplace law $\Delta P = 2\gamma_{\text{LV}}/R_0$ yields

$$P_0 = -\frac{2\Sigma_0}{R_0} = -\frac{2W \sin \theta_0}{L_0 (1 + \cos \theta_0)}. \quad (8)$$

B. The equations describing finite adhesion

Let us now consider the case of a finite contact potential W . The equilibrium shapes are those minimizing the sum of the bending free energy and the adhesion free energy, subject to the area and volume constraints. Considering axisymmetric shapes, we parameterize their contour by the tangent angle $\psi(s)$, where $s \in [0, s_1]$ is the arc-length (see Fig. 2), such that at $s = 0$ the membrane

leaves the substrate and at $s = s_1$ it attains the revolution axis. Although $\psi(s)$ alone is sufficient to describe the vesicle's shape, it is more convenient to also introduce the distance $r(s)$ to the revolution axis [23]. In the following, we shall denote by a dot derivation with respect to s . The two principal curvatures are $c_1 = \dot{\psi}$ (in the plane of Fig. 2) and $c_2 = (\sin \psi)/r$ (perpendicular to the plane of Fig. 2). Enforcing the constraints by Lagrange multipliers, the equilibrium shapes can be obtained by minimizing the following functional [23]:

$$F^*[r(s), \psi(s), s_1] = \pi r(0)^2 (\Sigma - W) + \int_0^{s_1} \mathcal{L}(r, \dot{r}, \psi, \dot{\psi}, \gamma) ds, \quad (9a)$$

where

$$\mathcal{L} = 2\pi r \left[\frac{1}{2} \kappa \left(\dot{\psi} + \frac{\sin \psi}{r} \right)^2 + \Sigma + \frac{P}{2} r \sin \psi \right] + 2\pi \gamma(s) (\dot{r} - \cos \psi). \quad (9b)$$

Here $\psi(s)$ and $r(s)$ are regular functions satisfying

$$\psi(0) = 0, \quad \psi(s_1) = \pi, \quad \text{and} \quad r(s_1) = 0, \quad (10)$$

while $r(0) \equiv L$ and s_1 are arbitrary. The above conditions are necessary for the vesicle's shape to be closed and in order to avoid discontinuities of the membrane's normal. The parameters Σ and P are the Lagrange multipliers associated with the area and volume constraints, respectively. The function $\gamma(s)$ is a field of Lagrange multipliers enforcing the condition $\dot{r} = \cos \psi$ for every s : this allows to treat $r(s)$ and $\psi(s)$ as independent functions in the first variation of F^* while ensuring that $r(s)$ and $\psi(s)$ effectively parameterize the same shape.

The first variation of F^* can be written as

$$\delta F^* = \int_0^{s_1} ds \left[\left(\frac{\partial \mathcal{L}}{\partial \psi} - \frac{d}{ds} \frac{\partial \mathcal{L}}{\partial \dot{\psi}} \right) \delta \psi(s) + \left(\frac{\partial \mathcal{L}}{\partial r} - \frac{d}{ds} \frac{\partial \mathcal{L}}{\partial \dot{r}} \right) \delta r(s) \right] + \delta F_b^*, \quad (11a)$$

with

$$\begin{aligned} \delta F_b^* &= \frac{\partial \mathcal{L}}{\partial \dot{\psi}}(s_1) \delta \psi(s_1) - \frac{\partial \mathcal{L}}{\partial \dot{\psi}}(0) \delta \psi(0) \\ &+ \frac{\partial \mathcal{L}}{\partial \dot{r}}(s_1) \delta r(s_1) - \frac{\partial \mathcal{L}}{\partial \dot{r}}(0) \delta r(0) \\ &+ 2\pi (\Sigma - W) r(0) \delta r(0) + \mathcal{L}(s_1) \delta s_1. \end{aligned} \quad (11b)$$

The membrane's equilibrium equations are obtained by setting to zero the coefficients of $\delta \psi(s)$ and $\delta r(s)$ in δF^* :

$$0 = \ddot{\psi} - \frac{\gamma \sin \psi}{\kappa r} - \frac{Pr \cos \psi}{2\kappa} + \frac{\dot{\psi} \cos \psi}{r} - \frac{\sin 2\psi}{2r^2}, \quad (12a)$$

$$0 = \dot{\gamma} - \frac{1}{2} \kappa \left(\dot{\psi}^2 - \frac{\sin^2 \psi}{r^2} \right) - \Sigma - Pr \sin \psi. \quad (12b)$$

The constraint $\dot{r} = \cos \psi$, which determines the Lagrange field $\gamma(s)$, constitutes actually a supplementary differential equation to be fulfilled. It is worth noticing that it can be obtained by varying F^* with respect to $\gamma(s)$, since

$$\frac{\partial \mathcal{L}}{\partial \gamma} - \frac{d}{ds} \left(\frac{\partial \mathcal{L}}{\partial \dot{\gamma}} \right) = 0 \quad \Leftrightarrow \quad \dot{r} = \cos \psi. \quad (13)$$

By analogy with Lagrangian mechanics, s playing the role of time, there exists therefore a conserved Hamiltonian \mathcal{H} , given by [23]

$$\begin{aligned} \mathcal{H} &= \mathcal{L} - \dot{\psi} \frac{\partial \mathcal{L}}{\partial \dot{\psi}} - \dot{r} \frac{\partial \mathcal{L}}{\partial \dot{r}} - \dot{\gamma} \frac{\partial \mathcal{L}}{\partial \dot{\gamma}} \\ &= 2\pi r \left[\frac{1}{2} \kappa \left(\dot{\psi}^2 - \frac{\sin^2 \psi}{r^2} \right) + \frac{\gamma}{r} \cos \psi - \Sigma - \frac{P}{2} r \sin \psi \right]. \end{aligned} \quad (14)$$

For an equilibrium solution, \mathcal{H} does not depend on s .

The boundary equilibrium equations are obtained by setting to zero the variation δF_b^* in Eq. (11b). Taking into account Eqs. (10) yields $\delta \psi(0) = 0$, $\delta \psi(s_1) = -\dot{\psi}(s_1) \delta s_1$ and $\delta r(s_1) = -\dot{r}(s_1) \delta s_1$. Therefore

$$\delta F_b^* = \mathcal{H}(s_1) \delta s_1 + 2\pi [(\Sigma - W) r(0) - \gamma(0)] \delta r(0). \quad (15)$$

Since δs_1 and $\delta r(0)$ are independent, we obtain

$$\mathcal{H}(s_1) = 0, \quad (16a)$$

$$(\Sigma - W) r(0) = \gamma(0). \quad (16b)$$

Since $\mathcal{H}(s)$ is a constant, Eq. (16a) implies $\mathcal{H}(0) \equiv \mathcal{H} = 0$. This yields $\frac{1}{2} \kappa \dot{\psi}^2(0) + \gamma(0)/r(0) - \Sigma = 0$. Hence the above conditions can be rewritten as

$$\mathcal{H} = 0, \quad (17a)$$

$$\frac{1}{2} \kappa \dot{\psi}^2(0) = W. \quad (17b)$$

Note that Eq. (17b) is the familiar curvature boundary condition for adhering membranes and thin elastic plates [14, 18]. Together with Eqs. (10), these equations form the boundary conditions of the problem. Note that we have 5 boundary conditions for a fourth-order system since s_1 is also an unknown.

C. First-order corrections to the limit W infinite

In order to compute the first-order corrections to the limit W infinite, we shall determine the shape of the contact angle region in the case of strong adhesion. To this aim, we first integrate once the membrane equilibrium equations by replacing Eq. (12b) by the integral condi-

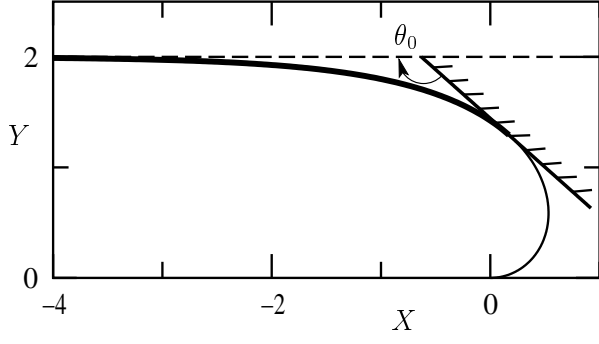


FIG. 3: Dimensionless universal shape of the contact angle region. For a given contact angle θ_0 , the actual shape, in units of $\ell = \sqrt{\kappa(1 + \cos \theta_0)}/W$, is the part of the curve comprised between the horizontal asymptote and the substrate, the latter being the tangent to the curve oriented at the angle θ_0 with respect to the asymptote.

tion $\mathcal{H} = 0$:

$$\ddot{\psi} = \frac{\gamma \sin \psi}{\kappa r} + \frac{Pr \cos \psi}{2\kappa} - \frac{\dot{\psi} \cos \psi}{r} + \frac{\sin(2\psi)}{2r^2}, \quad (18a)$$

$$\gamma = \frac{r}{\cos \psi} \left[\Sigma + \frac{P}{2} r \sin \psi - \frac{1}{2} \kappa \left(\dot{\psi}^2 - \frac{\sin^2 \psi}{r^2} \right) \right], \quad (18b)$$

$$\dot{r} = \cos \psi. \quad (18c)$$

1. Shape of the contact angle region

The equilibrium problem embodied in Eqs. (18) cannot be solved analytically. As evidenced by the boundary condition (17b), the width of the contact angle region (see Fig. 1) is of order $\sqrt{\kappa/W}$; hence the condition of strong adhesion can be expressed as

$$\epsilon = \frac{1}{L} \sqrt{\frac{\kappa}{W}} \ll 1, \quad (19)$$

where $L = r(0)$ is the adhesion disc's radius. This condition refines (3). We therefore start with the estimates:

$$\dot{\psi}(s) = \sqrt{\frac{W}{\kappa}} \times \mathcal{O}(1), \quad (20a)$$

$$r(s) = L_0 [1 + o(1)], \quad (20b)$$

$$\Sigma = \Sigma_0 [1 + o(1)], \quad (20c)$$

$$P = P_0 [1 + o(1)], \quad (20d)$$

where $o(1)$ indicates terms that tend to zero with ϵ and $\mathcal{O}(1)$ indicates terms of order unity. It follows that in Eq. (18b) all the terms in the brackets are equal to $W \times \mathcal{O}(1)$ except the last one which equals $W \times \mathcal{O}(\epsilon^2)$. We therefore neglect it, which amounts to neglecting the orthonormal principal curvature $(\sin \psi)/r$; thus Eq. (18b)

can be rewritten as

$$\gamma(s) = \frac{L_0}{\cos \psi} \left[\Sigma_0 + \frac{P_0}{2} L_0 \sin \psi - \frac{1}{2} \kappa \dot{\psi}^2 \right] [1 + o(1)]. \quad (21)$$

Plugging this expression of $\gamma(s)$ into Eq. (18a) and using Eqs. (20), we obtain

$$\ddot{\psi} = \left[\frac{\sin \psi}{\kappa \cos \psi} \left(-\frac{1}{2} \kappa \dot{\psi}^2 + \Sigma_0 + \frac{P_0 L_0}{2} \sin \psi \right) + \frac{P_0 L_0 \cos \psi}{2\kappa} - \frac{\dot{\psi} \cos \psi}{L_0} + \frac{\sin 2\psi}{2L_0^2} \right] [1 + o(1)]. \quad (22)$$

All the terms in this equation are equal to $W\kappa^{-1} \times \mathcal{O}(1)$, except the last two term which are equal to $W\kappa^{-1} \times \mathcal{O}(\epsilon)$ and $W\kappa^{-1} \times \mathcal{O}(\epsilon^2)$, respectively. Using the expressions of the zeroth-order Lagrange multipliers (7) and (8), we obtain finally

$$\ddot{\psi} = \left(-\frac{1}{2} \dot{\psi}^2 \tan \psi + \frac{W}{\kappa} \frac{\sin \psi - \sin \theta_0}{(1 + \cos \theta_0) \cos \psi} \right) [1 + o(1)]. \quad (23)$$

Neglecting the $o(1)$ term provides us with a simplified equation describing the contact angle region in the regime of strong adhesion. This equation can easily be integrated once by introducing the intermediate variable $\dot{\psi}^2/(2 \cos \psi)$ and using the boundary condition (17b):

$$\dot{\psi}^2 = \frac{2W}{\kappa} \frac{1 + \cos(\theta_0 + \psi)}{1 + \cos \theta_0}. \quad (24)$$

Its solution is

$$\psi(s) = 4 \arctan \left[\tanh \left(s \sqrt{\frac{W}{4\kappa(1 + \cos \theta_0)}} \right) \right] - \theta_0, \quad (25)$$

where we have shifted the arc-length s by a constant, the detachment point still corresponding to $\psi = 0$. Since the radius L of the adhesion disc has disappeared, the problem has actually become two-dimensional, as if the rim of the contact angle region were translationally invariant. This implies that in the present regime of strong but finite adhesion, the size of the vesicle has no influence on the shape of the contact angle region. Yet, the constraint on the reduced volume keeps an influence since it determines θ_0 .

Scaling lengths to $\ell = \sqrt{\kappa(1 + \cos \theta_0)}/W$, and introducing a normalized frame (X, Y) rotated of an angle θ_0 with respect to the frame (r, z) , the shape of the contact angle region assumes the universal expression:

$$X(S) = 2 \tanh S - S, \quad (26a)$$

$$Y(S) = 2 \left[1 - (\cosh S)^{-1} \right], \quad (26b)$$

where $S = s/\ell$ is the normalized arc-length. For a given contact angle θ_0 , the actual shape of the contact angle

region is obtained by putting the substrate tangent to this shape, at the angle θ_0 with respect to the horizontal asymptote of the curve, and then rescaling lengths with respect to ℓ , as shown in Fig. 3. This shape is the same as that found in [16], which was established using an open membrane description and by imposing the asymptotic direction of the membrane at the angle θ_0 through an externally imposed tension.

2. Contact angle extrapolation length

A useful characteristic of the contact angle region, used in RICM experiments in order to determine the ratio W/κ [17, 20], is the *extrapolation length* λ_1 (see Fig. 1). From the above calculation, valid in the regime of strong adhesion, we deduce

$$\lambda_1 \simeq \int_0^\infty \cos \psi \, ds - \int_0^\infty \frac{\sin \psi}{\tan \theta_0} ds = \sqrt{\frac{2\kappa}{W}} \cot \frac{\theta_0}{2}. \quad (27)$$

This expression holds even for deflated vesicles and agrees with the expression previously obtained in Ref. [17] for nearly spherical vesicles ($\pi - \theta_0 \ll 1$).

3. First-order corrections to the global observables

Let us determine, in the regime of strong but finite adhesion, the global observables characterizing the vesicle's shape: θ , R , L , H (see Sec. II for their definitions). To this purpose, we match the contact angle region to the rest of the vesicle. This is done by expressing the area and volume constraints:

$$A = A_{\text{cap}} - \delta A, \quad (28a)$$

$$V = V_{\text{cap}} - \delta V, \quad (28b)$$

where $A_{\text{cap}} = \pi R^2 [2(1 - \cos \theta) + \sin^2 \theta]$ is the area of the spherical cap osculatory to the vesicle plus the area of its bounding disc, $V_{\text{cap}} = \frac{1}{3} \pi R^3 [2(1 - \cos \theta) - \sin^2 \theta \cos \theta]$ is the volume enclosed by this spherical cap, and A and V are the actual vesicle's area and volume, respectively.

In the regime of strong adhesion, δA can be evaluated from the results of Sec. III C 1 by calculating the difference between the area associated with the approximate contact angle shape given by Eq. (25) and that associated with its asymptote:

$$\begin{aligned} \delta A &\simeq 2\pi L_0 \int_0^\infty ds - 2\pi L_0 \left(\lambda_1 + \int_0^\infty \frac{\sin \psi}{\sin \theta_0} ds \right) \\ &= 4\pi \left(\cos \frac{\theta_0}{2} - \cot \frac{\theta_0}{2} \right) \sqrt{\frac{2\kappa}{W}} L_0 = A \times \mathcal{O}(\epsilon), \end{aligned} \quad (29)$$

where $L_0 = R_0 \sin \theta_0$. As for $\delta V \approx \delta A \lambda_1$, it follows that it is equal to $V \times \mathcal{O}(\epsilon^2)$ since $\lambda_1 = L \times \mathcal{O}(\epsilon)$ [see Eq. (27)]. Note also that since in the limit $W \rightarrow \infty$ the vesicle's shape is actually a spherical cap, we have $A = A_{\text{cap}}(R_0, \theta_0)$ and $V = V_{\text{cap}}(R_0, \theta_0)$.

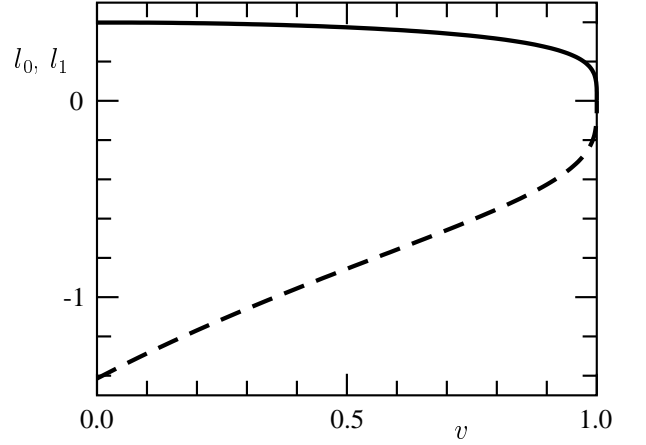


FIG. 4: Coefficients l_0 (solid line) and l_1 (dashed line) of the expansion (31a) of the radius L of the adhesion disc, as a function of the reduced volume v of the vesicle.

Setting $\theta = \theta_0 + \delta\theta$ and $R = R_0 + \delta R$, we obtain the first-order corrections $\delta\theta$ and δR by solving the system (28) to first order in ϵ . This yields

$$\delta\theta = \frac{2 \left(\sin \frac{\theta_0}{2} - 1 \right) (2 + \cos \theta_0)}{R_0 \sin \theta_0} \sqrt{\frac{2\kappa}{W}} + \mathcal{O}(\epsilon^2), \quad (30a)$$

$$\delta R = \frac{2 \left(1 - \sin \frac{\theta_0}{2} \right) \sin^2 \theta_0}{(1 - \cos \theta_0)^2} \sqrt{\frac{2\kappa}{W}} + \mathcal{O}(R_0 \epsilon^2). \quad (30b)$$

These results show that, in order to compensate the area cost δA of the contact angle region, the vesicle's shape flattens ($\delta R < 0$) with respect to the asymptotic case of infinite adhesion.

We are now able to determine the first-order corrections to L , the radius of the adhesion disc, and to H , the height of the vesicle. Since the intersection between the substrate and the osculatory spherical cap, described by (R, θ) , is a circle of radius $R \sin \theta$, we have $L \simeq R \sin \theta - \lambda_1$. Using Eqs. (30) and (27), L can be written in the dimensionless form:

$$\frac{L}{\sqrt{A}} = l_0 + l_1 \sqrt{\frac{\kappa}{WA}} + \mathcal{O}\left(\frac{\kappa}{WA}\right), \quad (31a)$$

with,

$$l_0 = \frac{L_0}{\sqrt{A}} = \sqrt{\frac{1 + \cos \theta_0}{\pi (3 + \cos \theta_0)}}, \quad (31b)$$

$$l_1 = -\sqrt{2} \frac{\cos \frac{\theta_0}{2}}{1 + \sin \frac{\theta_0}{2}}. \quad (31c)$$

Note that θ_0 is linked to the prescribed reduced volume v of the vesicle through expression (6). In Fig. 4 we have plotted l_0 and l_1 as a function of v .

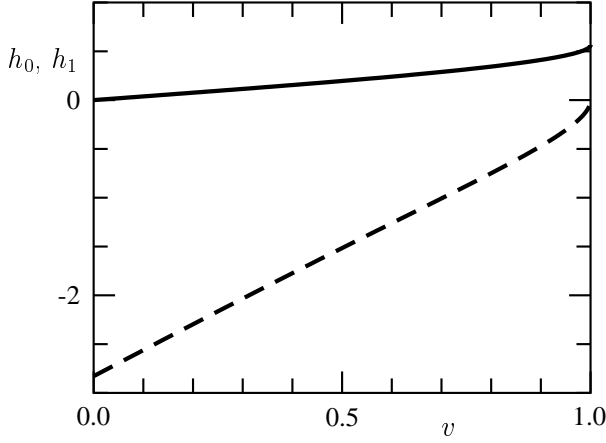


FIG. 5: Coefficients h_0 (solid line) and h_1 (dashed line) of the expansion (32a) of the total height of the vesicle, as a function of the reduced volume v of the vesicle.

As for H , since the osculatory spherical cap is tangent to the top of the vesicle, we have simply $H = R(1 - \cos \theta)$. Using Eqs. (30) we obtain

$$\frac{H}{\sqrt{A}} = h_0 + h_1 \sqrt{\frac{\kappa}{WA}} + \mathcal{O}\left(\frac{\kappa}{WA}\right), \quad (32a)$$

with,

$$h_0 = \frac{H_0}{\sqrt{A}} = \sqrt{\frac{1 - \cos \theta_0}{\pi(3 + \cos \theta_0)}}, \quad (32b)$$

$$h_1 = -2\sqrt{2} \left(1 - \sin \frac{\theta_0}{2}\right). \quad (32c)$$

The plots of h_0 and h_1 as a function of v are shown in Fig. 5. Note that h_0 and l_0 stem from simple geometrical considerations, while h_1 and l_1 originate from curvature elasticity effects.

4. Free energy of adhering vesicles

We now turn to the determination of the analytical development of the total free energy of the vesicle:

$$F = -\pi L^2 W + F_{\text{el}}, \quad (33)$$

where F_{el} is the curvature free energy. The latter is the sum of a contribution $F_{\text{el},1}$ arising from the contact-angle region and a contribution $F_{\text{el},2}$ arising from the top spherical cap. Since both the size and the curvature radius of the contact-angle region are of order $\sqrt{\kappa/W}$, $F_{\text{el},1}$ is of order $L\sqrt{\kappa/W} \times \kappa(\sqrt{W/\kappa})^2 = WL^2 \times \mathcal{O}(\epsilon)$. As for $F_{\text{el},2}$, it can be neglected since it is of order $\kappa \times \mathcal{O}(1) = WL^2 \times \mathcal{O}(\epsilon^2)$, as for a free vesicle.

In the strong adhesion regime, the orthoradial curvature $(\sin \psi)/r$ of the contact-angle region is negligible as

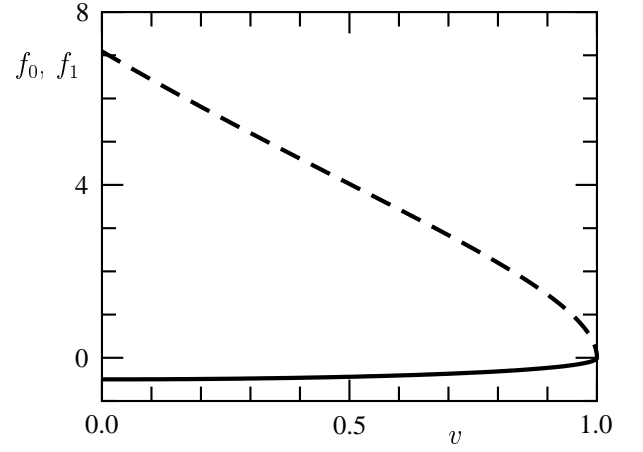


FIG. 6: Coefficients f_0 (solid line) and f_1 (dashed line) of the expansion (35a) of the free energy of the vesicle, as a function of the reduced volume v of the vesicle.

justified in Sec. III C 1. Therefore, using Eq. (24), we obtain

$$F_{\text{el}} \simeq \pi \kappa L_0 \int_0^\infty \psi^2 ds = 2\pi L_0 \sqrt{2\kappa W} \frac{1 - \sin \frac{\theta_0}{2}}{\cos \frac{\theta_0}{2}}. \quad (34)$$

Using the expression of L given by Eq. (31a), we finally obtain

$$\frac{F}{WA} = f_0 + f_1 \sqrt{\frac{\kappa}{WA}} + \mathcal{O}\left(\frac{\kappa}{WA}\right), \quad (35a)$$

with

$$f_0 = -\frac{1 + \cos \theta_0}{3 + \cos \theta_0}, \quad (35b)$$

$$f_1 = 8\sqrt{\pi} \frac{1 - \sin \frac{\theta_0}{2}}{\sqrt{3 + \cos \theta_0}}. \quad (35c)$$

The plots of f_0 and f_1 in terms of the reduced volume v are shown in Fig. 6.

As an application of this result, let us determine the force acting on an adhering vesicle in the presence of weak adhesion gradients: haptotaxis [21]. If the dynamical deformations during the movement are weak, the shape of the vesicle can be assimilated to its equilibrium shape on a substrate with a constant adhesion potential W equal to the average of W in the real adhesion disc. The force exerted on the vesicle is then

$$\begin{aligned} \mathbf{f} &= -\frac{\partial F}{\partial W} \nabla W \\ &= -\left[f_0 A + \frac{1}{2} f_1 \sqrt{\frac{\kappa A}{W}} + \mathcal{O}\left(\frac{\kappa}{W}\right) \right] \nabla W, \end{aligned} \quad (36)$$

where ∇ is the gradient on the substrate. Since f_0 and f_1 have opposite signs, the curvature elasticity decreases

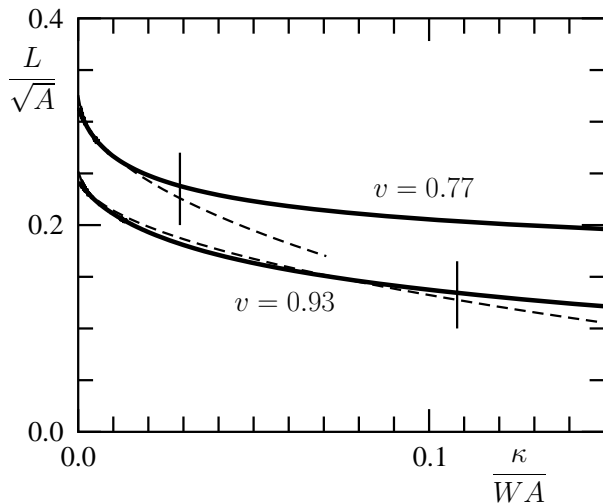


FIG. 7: Numerically calculated radius L of the adhesion disc as a function of $\kappa/(WA)$ (solid lines) for vesicles of reduced volume $v = 0.77$ and $v = 0.93$, along with its asymptotic expansion (31) (dashed lines). The vertical bars indicate the threshold at which the relative error between the exact value of L and its analytical estimate reaches 5%.

the haptotactic force with respect to the infinite adhesion limit. Moreover, for a given ∇W the haptotactic force is not constant but actually increases with W .

To check the order of magnitude of the haptotactic force, let us consider a $10\text{ }\mu\text{m}$ vesicle ($A \simeq 10^{-9}\text{ m}^2$) with $\kappa \simeq 10^{-19}\text{ J}$, subject to a contact potential varying uniformly from $W \simeq 10^{-4}\text{ mJ/m}^2$ to $W \simeq 10^{-3}\text{ mJ/m}^2$ on a distance $\simeq 1\text{ mm}$. Assuming a reduced volume $v = 0.77$ corresponding to $\theta_0 \simeq \pi/2$ [see Eq. (6)], we obtain a force varying from 0.26 pN to 0.29 pN (8% variation). With a simple Stokes law, this corresponds to velocities of the order of $1\text{ }\mu\text{m/s}$. Note that in infinite adhesion this gradient would give rise to a force equal to 0.3 pN .

IV. COMPARISON WITH THE EXACT NUMERICAL RESULTS

We expect the asymptotic expansions given in Secs. III C 3 and III C 4 to be accurate in the regime of strong adhesion. To check their validity, we have compared them with the exact values of the vesicle's observables, obtained by numerically integrating Eqs. (12) and (13).

In order to avoid numerical instabilities when approaching the axis of revolution ($r = 0$), we have chosen to integrate the equations starting from the top of the vesicle ($s = s_1$, see Fig. 2). To this aim, we impose the 4 initial conditions:

$$\mathcal{H}(s_1) = 0, \quad (37a)$$

$$r(s_1) = 0, \quad (37b)$$

$$\psi(s_1) = 0, \quad (37c)$$

$$\dot{\psi}(s_1) = c_0, \quad (37d)$$

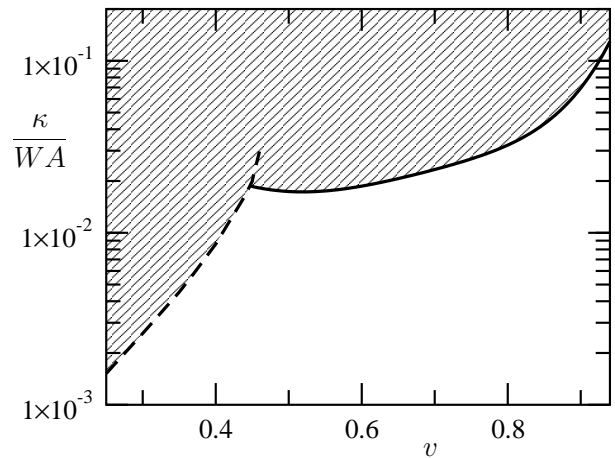


FIG. 8: White area: region of the $(v, \kappa/WA)$ plane where the analytical estimate of the radius L of the adhesion disc differs from its exact numerical evaluation by less than 5%. Above the dashed line (not fully shown) the axisymmetric oblate shapes correspond to an unphysical self-crossing of the membrane.

where $\mathcal{H}(s)$ is the first integral of the equilibrium equations given by Eq. (14) and c_0 is an arbitrary initial curvature. The integration proceeds backwards, starting from $s = s_1$ (the actual value of s_1 is arbitrary), and is stopped when $\psi = \pi$, meaning that the substrate has been reached. To span more easily all the values of the dimensionless parameter WA/κ for a given reduced volume v , we proceed as follows. For a given fixed value of the initial curvature c_0 , we vary the Lagrange multiplier Σ in Eqs. (12) until the solution has the desired reduced volume. During this search, the other Lagrange multiplier, P , is fixed to a value (positive for weakly adhering vesicles and negative for strongly adhering vesicles) assuring that the size of the vesicle is of order 1 in dimensionless units. Once the correct value of Σ has been obtained, we determine the area of the vesicle and its curvature at the point $\psi = \pi$, where it touches the substrate. The corresponding value of WA/κ is obtained through the boundary condition (17b). The set of all the solutions for a fixed v and all values of WA/κ corresponds to a trajectory in the (Σ, c_0) plane that has to be reconstructed by varying c_0 and Σ . Sometimes, a given c_0 corresponds to two or more values of Σ , which yields different values of WA/κ for the same reduced volume.

To exemplify our results, we show in Fig. 7 the radius L of the adhesion disc, as a function of the reduced inverse adhesion energy $\kappa/(WA)$, for vesicles of reduced volume $v = 0.77$ (or $\theta_0 \simeq \pi/2$) and $v = 0.93$. High adhesion energies correspond to low values of $\kappa/(WA)$, where our asymptotic formula (31) closely fits the exact numerical results. The vertical bars indicate the threshold above which the error associated with the analytical approximation is larger than 5%. At this threshold, L differs nonetheless from its infinite adhesion limit L_0 by more than 30%: significant deviations from the infinite adhesion limit are therefore predicted with a good precision

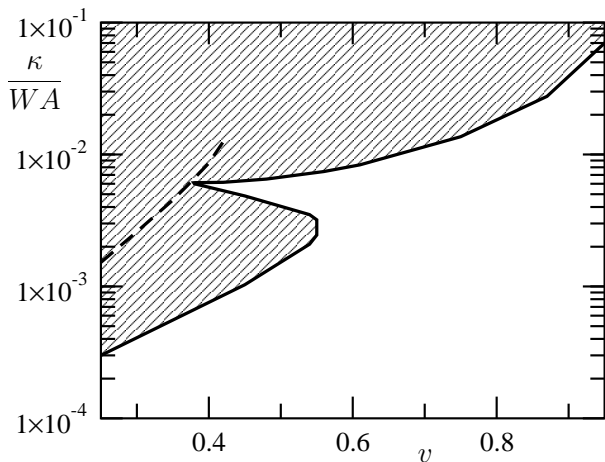


FIG. 9: Same as Fig. 8 but for the total height H of the vesicle.

by the asymptotic formula (31).

For vesicles of reduced volume in the range $0.25 \leq v \leq 0.95$, we have determined the threshold for $\kappa/(WA)$ at which the relative error between our analytical approximations and the exact results reaches 5%. In Fig. 8 we show this threshold for the adhesion disc's radius L , in Fig. 9 for the total vesicle's height H , and finally in Fig. 10 for the derivative dF/dW of the free energy with respect to the adhesion energy. The latter quantity is linked to the haptotactic force (36).

Typically, the 5% threshold occurs for values of $\kappa/(WA)$ comprised between 10^{-2} and 10^{-3} (see Figs. 8–10). Let us consider the case of “giant vesicles” since they are optically observable (typical size $\simeq 10\text{--}100\ \mu\text{m}$). Supposing an area of $\simeq 10^3\ \mu\text{m}^2$ and a bending rigidity $\kappa \simeq 10^{-19}\text{ J}$, the 5% threshold occurs for values of W in the weak adhesion range $10^{-5}\text{--}10^{-4}\text{ mJ/m}^2$. Our analytical estimates seem therefore able to describe the adhesion of giant vesicles up to the lowest values of W experimentally accessible. For smaller vesicles, the threshold is more limitative, as it corresponds to higher adhesion energies W . Note also that in the case of weak adhesion, the picture could be quantitatively different for vesicles filled with a fluid denser than the outside medium, because of gravity effects.

V. DISCUSSION AND POSSIBLE APPLICATIONS

Taking into account the effect of membrane elasticity to first-order in $\sqrt{\kappa/(WA)}$, we have analytically determined the global observables characterizing adhering vesicles. Our calculation is based on the fact that if adhesion prevails over elasticity, most of the elastic contributions to the free energy are located in the “contact angle region.” We have numerically determined the region of validity of our analytical expansions, in the $(v, \kappa/(WA))$

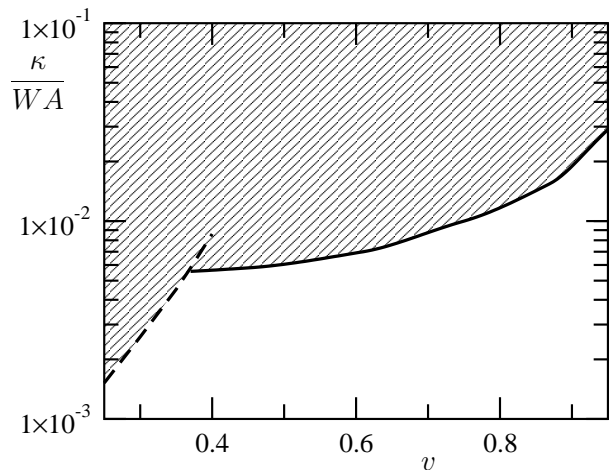


FIG. 10: Same as Fig. 8 but for the derivative dF/dW of the free energy of the vesicle with respect to the adhesion energy W .

parameter space, corresponding to a 5% maximum error. It turns out that for “giant vesicles” (typical radius $10\text{--}100\ \mu\text{m}$), this region comprises practically all the accessible adhesion surface energies W . Besides, our analytical estimates correctly describe significant deviations with respect to the infinite adhesion limit.

We have throughout assumed that the area A and volume V of the vesicle were strictly fixed, while vesicles actually possess small but finite stretching elasticity and osmotic compressibility. It is easily shown, however, that a self-consistent choice of the Lagrange multipliers Σ and P yields the same equilibrium solution in the presence of arbitrary stretching and osmotic potentials. It follows that our expressions of $\delta\theta$, δR , L and H remain correct provided that A and V are the actual area and volume (that now depend on W).

Measurements of the contact potential W are usually performed by RICM imaging of the contact angle region [17, 20]. The value of W is inferred either from the local curvature $\dot{\psi}(0)$ through Eq. (17b), or from the extrapolation length λ_1 through Eq. (27) (an approximated formula valid for $\pi - \theta_0 \ll 1$ is actually used [17]). The precision of the former measurement is limited by the fact that the vesicle's curvature varies abruptly close to its detachment point, the exact position of which is always slightly ambiguous. The extrapolation length measurement relies on the existence of a well defined asymptote of the vesicle's profile close to the contact angle region: it is therefore suitable only for the strongest adhesions. The expressions of L and H found in Sec. III C 3 allow to envisage novel measurements of W , based on *global* characteristics of the adhering vesicle. To this aim, one needs to know also the vesicle's total area and volume. They can be either directly determined by imaging a side view of the vesicle [24], or inferred by osmotically deflating a spherical vesicle of known radius in a controlled way. The fact that W can be determined through two independent

measurements (L and H) allows to better estimate the experimental errors and to validate the model. Moreover, such global measurements are complementary to the above-cited local ones, since they are more adapted for measuring weaker values of W . The precision of the measurement should increase as W decreases, as long as one remains inside the authorized zone of Figs. 8 and 9. In fact, for W too strong, L and H saturate, while for W too weak the analytical expansions of L and H lose their validity. However, as we have seen, the low W limitation is not relevant for “giant vesicles”.

Finally, the haptotactic force (36) suggests the possibility to determine the size of suboptical vesicles by measuring their velocity of migration on a substrate presenting a controlled adhesion gradient, supposing a linear viscous friction law. Fitting the evolution of the vesicle's velocity as a function of W allows to determine the vesicle's area and volume, provided that the dependence of the friction coefficient on $\kappa/(WA)$ and v is known. The latter could be determined using giant vesicles of known area and volume.

-
- [1] J. Israelachvili, *Intermolecular & Surface Forces* (Academic Press, New York, 1991).
 - [2] B. Sternberg, J. Grumpert, G. Reinhardt, and K. Gawrisch, *Biochim. Biophys. Acta* **898**, 223 (1987).
 - [3] M.-A. Guedeau-Boudeville, L. Jullien, and J.-M. di Meglio, *Proc. Natl. Acad. Sci. USA* **92**, 9590 (1995).
 - [4] A.-L. Bernard, M.-A. Guedeau-Boudeville, L. Jullien, and J.-M. di Meglio, *Langmuir* **16**, 6809 (2000).
 - [5] C. A. Keller, K. Glasmästar, V. P. Zhdanov, and B. Kasemo, *Phys. Rev. Lett.* **84**, 5443 (2000).
 - [6] E. Sackmann, *Science* **271**, 43 (1996).
 - [7] R. Bruinsma, A. Berisch, and E. Sackmann, *Phys. Rev. E* **61**, 4253 (2000).
 - [8] U. Seifert, *Advances in Physics* **46**, 13 (1997).
 - [9] J. O. Rädler, T. J. Feder, H. H. Strey, and E. Sackmann, *Phys. Rev. E* **51**, 4526 (1995).
 - [10] H. Helfrich, *Z. Naturforsch.* **28C**, 693 (1973).
 - [11] C.-H. Lee, W.-C. Lin, and J. Wang, *Phys. Rev. E* **64**, 020901(R) (2001).
 - [12] S. Svetina, A. Ottova-Lietmannova, and R. Glaser, *J. Theor. Biol.* **94**, 13 (1982).
 - [13] U. Seifert, L. Miao, and H. G. Döbereiner, *Springer Proceedings in Physics* **66**, 93 (1992).
 - [14] U. Seifert and R. Lipowsky, *Phys. Rev. A* **42**, 4768 (1990).
 - [15] P.-G. de Gennes, *Rev. Mod. Phys.* **57**, 827 (1985).
 - [16] R. M. Servuss and W. Helfrich, *J. Phys. France* **50**, 809 (1989).
 - [17] Z. Guttenberg, A. R. Bausch, B. Hu, R. Bruinsma, L. Moroder, and E. Sackmann, *Langmuir* **16**, 8984 (2000).
 - [18] L. Landau and E. Lifchitz, *Théorie de l'Élasticité* (Mir, Moscou, 1967).
 - [19] R. Rosso and E. G. Virga, *Proc. R. Soc. Lond. A* **455**, 4145 (1999).
 - [20] J. Nardi, R. Bruinsma, and E. Sackmann, *Phys. Rev. E* **58**, 6340 (1998).
 - [21] I. Cantat, C. Misbah, and Y. Saito, *Eur. Phys. J. E* **3**, 403 (2000).
 - [22] D. J. Struik, *Lectures on Classical Differential Geometry* (Dover Publications, New York, 1961).
 - [23] U. Seifert, K. Berndl, and R. Lipowsky, *Phys. Rev. A* **44**, 1182 (1991).
 - [24] M. Abkarian, C. Lartigue, and A. Viallat, *Phys. Rev. E* **63**, 041906 (2001).